Red-Shifted Carrier Multiplication Energy Threshold and Exciton Recycling Mechanisms in Strongly Interacting Silicon Nanocrystals

Ivan Marri,*,[†] Marco Govoni,*,[‡,#] and Stefano Ossicini[†]

[†]Department of Science and Methods for Engineering (DISMI), University of Modena and Reggio Emilia, via Amendola 2, Pad. Morselli, 42122 Reggio Emilia, Italy

[‡]Department of Physics, University of Modena and Reggio Emilia, via Campi 213/a, 41125 Modena, Italy

S *Supporting Information*

ABSTRACT: We present density functional theory calculations of carrier multiplication properties in a system of strongly coupled silicon nanocrystals. Our results suggest that nanocrystal–nanocrystal interaction can lead to a reduction of the carrier multiplication energy threshold without altering the carrier multiplication efficiency at high energies, in agreement with experiments. The time evolution of the number of electron–hole pairs generated in a system of strongly interacting nanocrystals upon absorption of high-energy photons is analyzed by solving a system of coupled rate equations, where exciton recycling mechanisms are implemented. We reconsider the role played by Auger recombination which is here accounted also as an active, nondetrimental process.
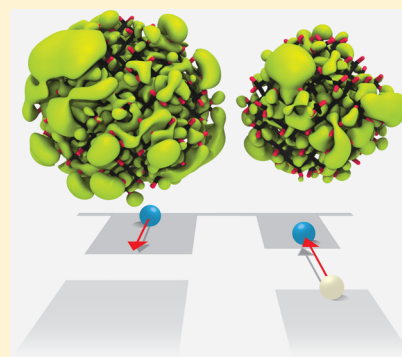
INTRODUCTION

The possibility of fully exploiting solar radiation for photovoltaic (PV) applications represents one of the most important topics of the modern research. In this context, the recent and impressive development in the field of nanotechnologies and the discovery of new nanomaterials have opened important prospectives for the realization of innovative solar cells that can reach high performances also when cheap and low-grade nanomaterials are employed. Optoelectronic properties of nanocrystalline solar cells can be tuned to increase the percentage of sunlight frequencies available for photocurrent conversion by manipulating nanocrystals (NCs) size, shape, passivation, and doping.[1−6] In these systems, enhancement of the carrier–carrier Coulomb interaction induced by quantum confinement promotes the occurrence of nondissipative decay processes like the carrier multiplication (CM) effect. CM is a Coulomb-driven nonradiative decay process that results in the generation of several e−h pairs after absorption of a single high-energy photon. When CM is effective, the excess energy is not lost into heat but can be used in the photoconversion process. Effects induced by CM on excited carriers dynamics have been observed by ultrafast spectroscopy in a wide range of systems, such as PbSe and PbS,[7−19] CdSe and CdTe,[15,20−22] PbTe,[23] InAs,[24,25] InP[26] and Si,[27] despite the fact that in some cases such effects have been overestimated due to the occurrence of photocharging processes.[28−30] For what concerns theoretical investigations, CM was modeled for isolated NCs by implementing three different schemes, that is the first-order perturbation theory (impact ionization),[31−38] the second-order perturbation theory (weak coupling limit),[39,40] and the coherent superposition of single and multiexcitonic states

(strong coupling limit).[41] Experimental and theoretical efforts have been focused on both the study of the microscopic properties of the CM dynamics and on the research of new nanomaterials where nanostructures are engineered and organized to maximize the overall efficiency of CM and to extend its relevance for PV applications. In this context, promising results have been obtained using systems of closely packed NCs, in particular dense arrays of Si-NCs[42−44] and systems of strongly coupled PbSe quantum dots.[45,46] In both these systems, a CM energy threshold reduction was observed when NCs were placed in close proximity, pointing out that a broader portion of the solar spectrum can be made able to activate efficient CM dynamics when NCs strongly interact. Currently, a microscopic interpretation of this effect is still missing. Formation of multiexciton configurations distributed on space-separated nanostructures, moreover, was hyphothesized to explain results obtained in induced absorption (IA) measures conducted in the system of closely packed Si-NCs.[44] In this experiment, consisting of pumping the sample and probing it after some delay time, photogenerated carrier densities were monitored as a function of the energy of the adsorbed photon, and the IA dynamics were recorded to discern localization of generated e−h pairs. The observed effect, originated by NCs interplay, leads to the generation of Auger-unaffected long-lived e−h pairs and favors carrier extraction in nanostructured solar cell devices. Under a theoretical point of view, effects induced by NC−NC interaction on CM dynamics were investigated by Govoni et al.[37] who quantified, for the first
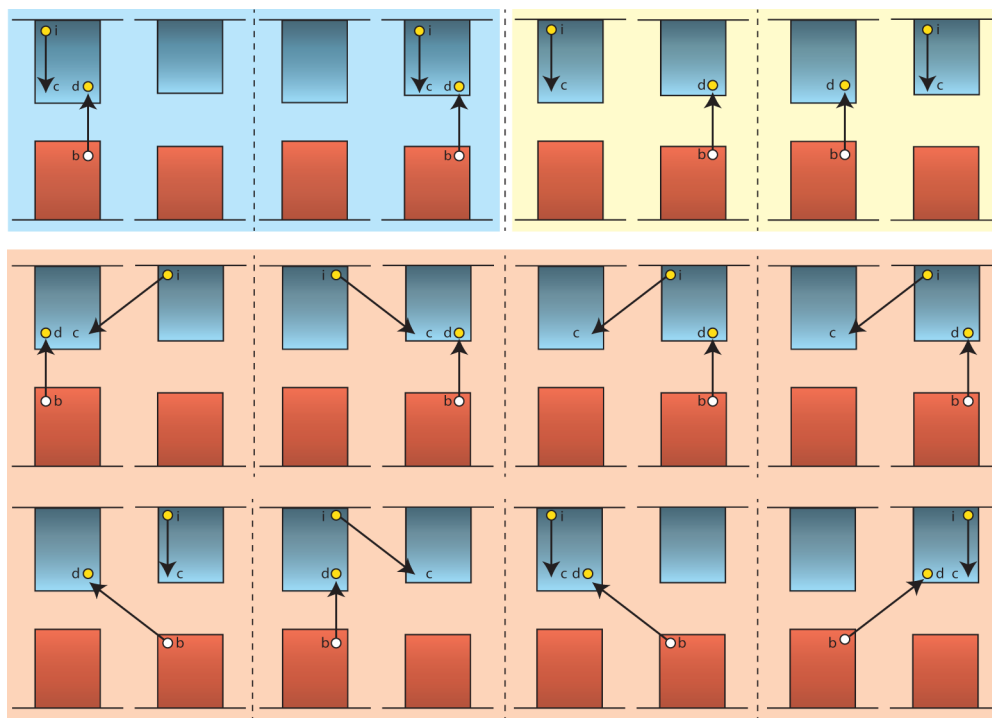
Figure 1. Schematic representation of one-site CM processes (blue panel), and two-site CM processes (SSQC: yellow panel, CDCT: orange panel) is reported in the figure for the generic transition $(i,b) \rightarrow (c,d)$. We show only mechanisms ignited by a relaxing electron (hole spectator).

time by ab initio calculations, both one- and two-site CM lifetimes (the first ones account for transitions which involve initial and final states localized onto the same NC, whereas the second ones account for mechanisms where initial and final states are localized onto different NCs). Two-site CM processes were further divided into energy transfer CM effects, termed space separated quantum cutting (SSQC), and Coulomb driven charge transfer (CDCT), see Figure 1. After defining a CM lifetime hierarchy ($\tau_{\text{one-site}} < \tau_{\text{CDCT}} < \tau_{\text{SSQC}}$), conditions that maximize both SSQC and CDCT mechanisms were explained on the basis of the so-called wave function sharing regime.

■ METHOD

In this work we go beyond results of ref 37 by analyzing new and crucial aspects of CM dynamics induced by NCs interplay. To this purpose, we analyze a prototype system formed by two-interacting Si-NCs, (the $Si_{293}H_{172} \times Si_{147}H_{100}$) placed at a tunable separation. In our approach, electronic properties are calculated from first-principles within the density functional theory (DFT) adopting a supercell approach in the reciprocal space. CM dynamics are then described as an impact ionization process that follows the primary photoexcitation event, that is by applying first-order perturbation theory to Kohn–Sham (KS) states. Here, the decay of an exciton into a biexciton is described as the sum of two processes: the relaxation of an electron into a negative trion (two electrons and a hole) and the relaxation of a hole into a positive trion (two holes and an electron).[32,36] CM lifetimes for mechanisms ignited by a relaxing electron (eq 1) or by a relaxing hole (eq 2) are calculated by applying the Fermi's golden rule as a function of the energy E_i of the relaxing carrier (energy of the initial state):

$$\tau^e_{n_i,\mathbf{k}_i}(E_i) = \left[\sum_{n_c,n_d}^{\text{cond.}} \sum_{n_b}^{\text{val.}} \sum_{\mathbf{k}_b,\mathbf{k}_c,\mathbf{k}_d}^{\text{1BZ}} 4\pi[|M_D|^2 + |M_E|^2 \right.$$
$$\left. + |M_D - M_E|^2] \delta(E_i + E_b - E_c - E_d) \right]^{-1} \quad (1)$$

$$\tau^h_{n_i,\mathbf{k}_i}(E_i) = \left[\sum_{n_c,n_d}^{\text{val.}} \sum_{n_b}^{\text{cond.}} \sum_{\mathbf{k}_b,\mathbf{k}_c,\mathbf{k}_d}^{\text{1BZ}} 4\pi[|M_D|^2 + |M_E|^2 \right.$$
$$\left. + |M_D - M_E|^2] \delta(E_i + E_b - E_c - E_d) \right]^{-1} \quad (2)$$

Here indexes i, b, c, and d identify states involved in the transition (see Figure 1), n and $\mathbf{k}$ denote DFT KS states, 1BZ is the first Brillouin zone and M_D and M_E are the direct and exchange screened Coulomb matrix elements. These latter are calculated in reciprocal space among KS states by solving the Dyson's equation in the random phase approximation[47,48] (see Supporting Information [SI] for details). Energy conservation is guaranteed by the delta function. CM rates are calculated as the reciprocal of the lifetimes. Equations 1 and 2 are keeping track of the initial state and involve a sum over all possible final states. They hold for any system of NCs, regardless of the presence of a mutual interaction among them.

When NCs are placed in close proximity, wave functions can delocalize over both nanostructures. We therefore introduce a new parameter s_x, termed spill-out, that defines the percentage of localization of a generic KS electronic state $n_x\mathbf{k}_x$ onto a well-selected NC. This parameter is arbitrarily set to zero (one) when the state $n_x\mathbf{k}_x$ is completely localized on the largest (smallest) NC and takes values between zero and one when $n_x\mathbf{k}_x$ is shared among the two NCs (see SI). A general definition of the one- and two-site CM rates, that holds for systems of both isolated and interacting NCs, is reported below as a function of the energy of the initial carrier,

$$\frac{1}{\tau^{e/h}_{\text{one-site}}(E_i)} = \sum_{n_b\mathbf{k}_b} \sum_{n_c\mathbf{k}_c} \sum_{n_d\mathbf{k}_d} [s_{n_i\mathbf{k}_i} s_{n_b\mathbf{k}_b} s_{n_c\mathbf{k}_c} s_{n_d\mathbf{k}_d}$$
$$+ (1 - s_{n_i\mathbf{k}_i})(1 - s_{n_b\mathbf{k}_b})(1 - s_{n_c\mathbf{k}_c})(1 - s_{n_d\mathbf{k}_d})] \frac{1}{\tau^{e/h}_{(i,b)\rightarrow(c,d)}(E_i)}$$
$$(3)$$

$$\frac{1}{\tau^{e/h}_{\text{two-site}}(E_i)} = \frac{1}{\tau^{e/h}_{n_i\mathbf{k}_i}(E_i)} - \frac{1}{\tau^{e/h}_{\text{one-site}}(E_i)} \quad (4)$$

where $\tau^{e/h}_{\text{one-site}}(E_i)$ and $\tau^{e/h}_{\text{two-site}}(E_i)$ are the one- and two-site CM lifetimes, respectively. In eq 4, the sum is performed over all the
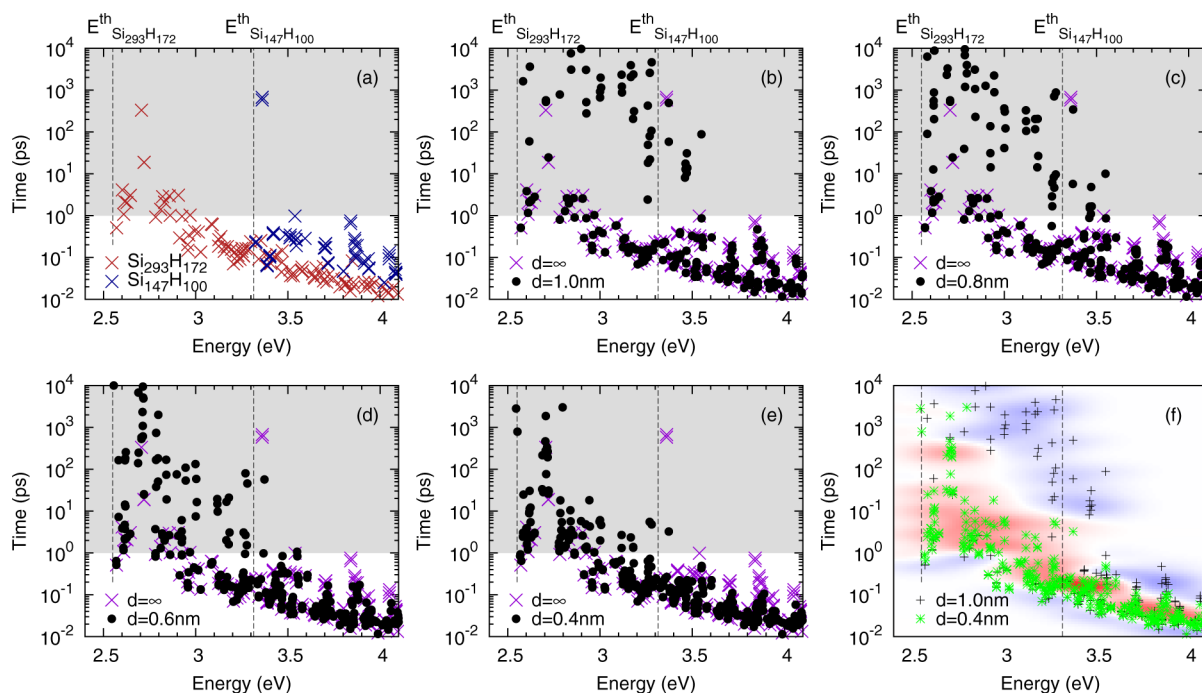
Figure 2. Calculated CM lifetimes for the system $Si_{293}H_{172} \times Si_{147}H_{100}$ are reported as a function of the NC−NC separation and of E_i. The considered NCs have a diameter of about 2.4 and 1.9 nm and an energy gap of 1.70 and 2.21 eV, respectively. CM lifetimes have been calculated by omitting vacuum states. In panel (a), NC−NC interaction is turned off (we simulate a system where NCs are placed at high distance, configuration labeled with $d = \infty$). Red (blue) crosses identify calculated CM lifetimes for the isolated $Si_{293}H_{172}$ ($Si_{147}H_{100}$). The zero of the energy is placed at half gap, and therefore $E^{th}_{Si_{293}H_{172}} = 2.55$ eV and $E^{th}_{Si_{147}H_{100}} = 3.32$ eV. From panel (b) to panel (e), calculated CM lifetimes for $d = 1.0, 0.8, 0.6,$ and 0.4 nm are reported (black points). NC−NC separation is calculated as the shortest distance between NCs surface atoms. Purple crosses keep track of the calculated CM lifetimes for the isolated Si-NCs. The difference between the distributions obtained by covering each point of the plots (e) and (b) with a 2D Gaussian function is reported in the panel (f). A colored scale is adopted to point out effects induced by NCs interplay when we move from a configuration of weakly (panel b) to a configuration of strongly (panel e) interacting NCs. Red (blue) zones emphasize regions where the number of CM decay paths increase (decrease) as a consequence of the NC−NC distance reduction. Green stars (black crosses) keep track of the calculated CM lifetimes at $d = 0.4$ (1.0) nm.

possible final states and $1/\tau^{e/h}_{(i,b)\to(c,d)}(E_i)$ is the total CM rate for the specific single transition $(i,b) \to (c,d)$ (see Figure 1). The weighting factors $s_{n_i k_i}$, $s_{n_b k_b}$, $s_{n_c k_c}$, and $s_{n_d k_d}$ are the spill-out parameters of the states i, b, c and d involved in the CM decay process. When all these parameters are zero (one), that is when $s_{n_i k_i} = 0$, $s_{n_b k_b} = 0$, $s_{n_c k_c} = 0$, and $s_{n_d k_d} = 0$ ($s_{n_i k_i} = 1$, $s_{n_b k_b} = 1$, $s_{n_c k_c} = 1$, and $s_{n_d k_d} = 1$), states involved in the CM transition are completely localized on the $Si_{293}H_{172}$ ($Si_{147}H_{100}$), and the total CM rate is completely given by one-site processes. In other cases, the total CM rate shows both one-site and two-site CM character.

RESULTS AND DISCUSSIONS

Calculated CM lifetimes for mechanisms promoted by a relaxing electron (eq 1) are reported in Figure 2 as a function of both the energy E_i and of the NC-NC separation d (similar results can be obtained for processes ignited by a relaxing hole, eq 2). In panel (a), calculated CM lifetimes for the isolated $Si_{293}H_{172}$ (red crosses) and $Si_{147}H_{100}$ (blue crosses) are depicted. This panel represents an ideal configuration comprising sparse arrays of Si-NCs where interaction between nanostructures can be neglected. In panels (b−e), calculated CM lifetimes for interacting NCs are reported, with a NC−NC separation d that is reduced from 1.0 to 0.4 nm, by steps of 0.2 nm. Noticeably, NCs interplay can activate new CM decay paths (that is processes that, due to the energy conservation law, cannot occur in systems of noninteracting NCs) or can, by adding new contributions, make more complicated CM

dynamics that already exist in systems of noninteracting NCs. Black circle dots of panels (b−e) can be therefore induced by occurrence of purely one-site CM mechanisms or of purely two-site CM processes or can account for the simultaneous combination of one- and two-site CM events, regardless of their relative weight. The theoretical CM activation energies $E^{th}_{Si_{293}H_{172}}$ and $E^{th}_{Si_{147}H_{100}}$ are obtained by multiplying by a factor of 2 the NCs energy gaps and represent ideal lower limits for the detectable CM energy thresholds. This latter defines the energy at which CM effects become measurable, that is when CM decay processes become faster than all other competitive relaxation mechanisms.[49−51] Obviously a detailed determination of the CM energy threshold requires a precise estimation of the thermalization time. Unfortunately, due to the huge numerical resources required, a detailed ab initio calculation of such processes represents currently, for the considered systems, an unattainable task. However, for Si-NCs, non-CM relaxation times are expected to be of the order of $1 \div 10$ ps.[52,53] These lifetimes will be taken as a reference for thermalization mechanisms and will be compared with the ones calculated for the CM decay dynamics. Starting from this consideration, we purposely divide results of Figure 2 (from panel (a) to panel (e)) in two parts: a region that counts subpicosecond CM decay processes (ultrafast CM events) and a shared region that accounts for near CM-threshold dynamics and that comprises CM decay paths with a lifetime ≥ 1 ps. Of this latter, we essentially analyze the dependence on NC−NC separation of
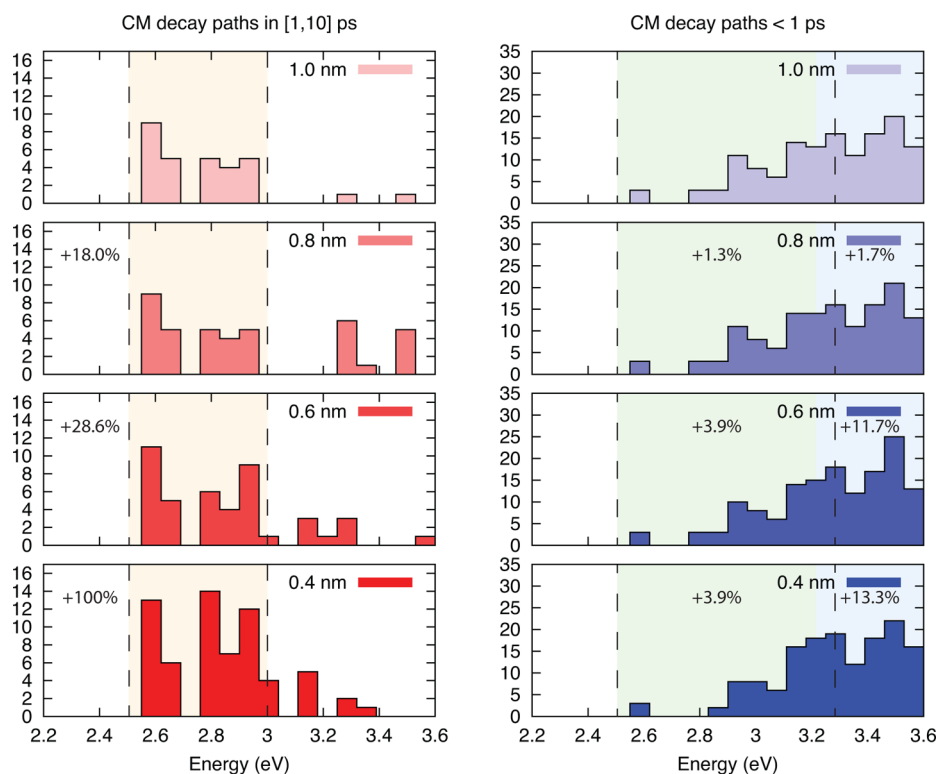
Figure 3. Distribution of the number of CM decay events that occur with lifetimes between $1 \div 10$ (<1) ps is reported in the left panel (right panel) as a function of the energy of the initial state E_i. Moving from the topmost panel to the bottommost panel we consider the cases $d = 1.0, 0.8, 0.6$, and 0.4 nm. As a reference, $E^{th}_{Si_{293}H_{172}} = 2.55$ eV eV and $E^{th}_{Si_{147}H_{100}} = 3.32$ eV. Colored zones identify specific regions of the plots. For each of them, the increment of the number of CM decay paths with respect to the ones recorded at $d = 1$ nm, is reported. Our results point out that, in the range of energies $E^{th}_{Si_{293}H_{172}} \div 3.0$ ($E^{th}_{Si_{147}H_{100}}$) eV and lifetimes $1 \div 10$ ps, the number of CM decay paths increases by 18.0% (34.5%) when d is reduced from 1.0 to 0.8 nm, by 28.6% (48.3%) when d is reduced from 1.0 to 0.6 nm, and by 100% (117.2%) when d is reduced from 1.0 to 0.4 nm. Less important changes are instead recorded when subps processes are analyzed. Here the percentage of the increment is reported for energies between $E^{th}_{Si_{293}H_{172}} \div E^{th}_{Si_{147}H_{100}}$ and for energies greater than $E^{th}_{Si_{147}H_{100}}$.

the decay paths that are sufficiently fast to compete with non-CM relaxation dynamics and that are therefore fundamental to determine the CM energy threshold (range of lifetimes, $1 \div 10$ ps). Results reported in panel (a) describe CM dynamics in a system of independent, noninteracting, Si-NCs. Results of panel (b), instead, refer to CM dynamics in a system of weakly interacting Si-NCs. Here, new CM decay events are induced by NCs interplay, and new points appear in the CM lifetime plot. In spite of this, however, the typical tracks of the CM dynamics of the isolated NCs remain clearly identifiable. In this configuration, NC−NC interaction is weak, and the quantum confinement imposed by hydrogen passivation strongly limits wave functions delocalization and hence the relevance of two-site CM processes. As a consequence at $d = 1$ nm, additional contributions induced by NCs interplay on CM poorly modify carrier relaxation dynamics. When NC−NC separation is further reduced, important changes emerge in both the number and the distribution of points of Figure 2 (panels (c−e)). Such changes concern essentially transitions that fall in the shared region with energies between $E^{th}_{Si_{293}H_{172}}$ and $E^{th}_{Si_{147}H_{100}}$. Two different effects simultaneously appear when d decreases: (i) new points are induced in the CM lifetimes plots as consequence of the occurrence of new CM decay paths, (ii) a large number of points move toward slower CM lifetimes. As a final result, at $d = 0.4$ nm, calculated CM lifetimes for the $Si_{293}H_{172} \times Si_{147}H_{100}$ resemble the ones of the isolated $Si_{293}H_{172}$ NC although, especially at low energies, CM is now made more

intense by the presence of a larger number of CM decay paths. The typical CM dynamics recorded for the isolated $Si_{147}H_{100}$ near $E^{th}_{Si_{147}H_{100}}$, that are well recognizable at $d > 0.8$ nm, are now largely missing. At $d = 0.4$ nm the system of two interacting NCs behaves as a unique structure where characteristics of the individual components are completely lost. Additional information on the role played by NCs interplay on CM dynamics can be obtained by replacing the discrete distribution of points of Figure 2 (panels (a−e)) with a continuous function that, for all the considered NC−NC separations, is calculated by covering each point of the plot with a 2D Gaussian; the obtained contributions are then added together on the entire window of permitted energies and lifetimes. The difference between the distributions calculated for $d = 0.4$ nm and $d = 1.0$ nm are reported in panel (f). Here red (blue) parts of the plot are associated with an increment (decrement) in the number of CM decay paths. As a consequence of the reduced NC−NC separation, we record an augmented number of CM decay paths in a region of the plot that resembles the one traced by the $Si_{293}H_{172}$ (see Figure 2, red cross-type points of panel (a)), that is the NC with low energy gap and low CM energy threshold. As pointed out by histograms of Figure 3, where the number of CM decay paths is counted as a function of d and E_i for transitions with lifetimes that fall in the range $1 \div 10$ ps (left panels) or in the subpicosecond (subps) region (right panels), such increments are particularly marked for energies between
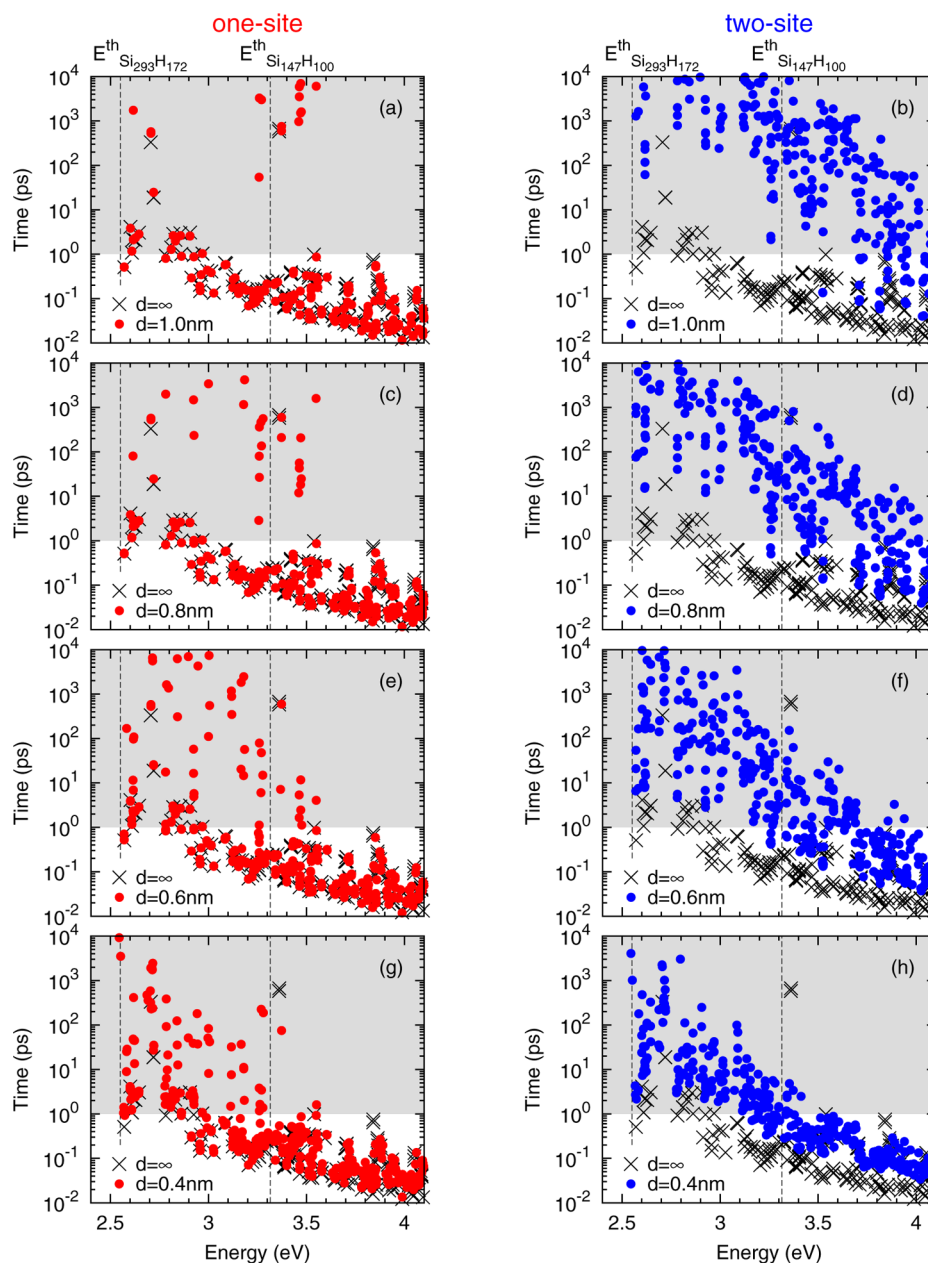
Figure 4. One-site CM lifetimes (left panels, red points) and two-site CM lifetimes (right panels, blue points) are reported in the figure as a function of the NC−NC separation. Cross-type points keep track of the CM lifetimes calculated for the system of noninteracting NCs ($d = \infty$).

$E_{Si_{293}H_{172}}^{th} \div E_{Si_{147}H_{100}}^{th}$ and lifetimes between $1 \div 10$ ps. In particular at $d = 0.4$ nm, in the range $2.55 \div 3.0$ eV, we count a double number of CM decay processes with respect to the ones recorded at $d = 1.0$ nm. When NCs strongly interact, therefore, we observe a non-negligible intensification of CM dynamics at low energies with respect to the one recorded for the equivalent system of weakly interacting NCs. This effect is very important and can lead to a red-shift of the detectable energy threshold, thus explaining the CM energy threshold reduction observed in different systems of closely packed NCs.[44,46] A different behavior is instead detected when subps CM decay paths are analyzed (right panels of Figure 3). Due to the fact that CM lifetimes monotonically decrease with respect to E_i, such transitions are in general induced by relaxation processes from high-energy states. As pointed out by results of panel (f) of Figure 2, NCs interplay modifies CM dynamics also when high-

energy decay processes are taken into account. Such changes, however, are drastically less important than the ones recorded at low energies. For instance, for the subps CM decay paths that occur above $E_{Si_{147}H_{100}}^{th}$, we detect a variation by 13% only when d is moved from 1.0 to 0.4 nm. Our results, therefore, point out that CM benefits from the NCs interplay especially at low energies, where NC−NC interaction leads to a significant intensification of the CM dynamics and thus to a possible reduction of the detectable CM energy threshold. Far from the activation threshold, instead, the occurrence of new CM processes driven by NCs interplay does not lead to a significant intensification of the CM dynamics. As a result, for the considered systems, CM energy threshold and CM efficiency at high energies are not correlated, on the contrary of what is expected for isolated NCs.[17] Noticeably, a similar result was highlighted by measurements conducted on closely packed
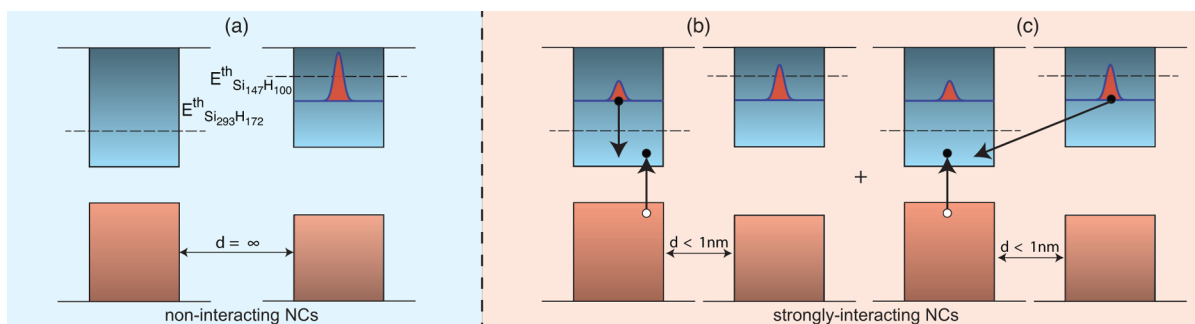
Figure 5. On the left, a system of two noninteracting NCs is depicted. An electronic state with energy between $E^{th}_{Si_{293}H_{172}}$ and $E^{th}_{Si_{147}H_{100}}$ localized onto the $Si_{147}H_{100}$ is shown. For the energy conservation law, CM recombination processes are not permitted from this state. On the right, a system of strongly interacting NCs is reported. The electronic state is now delocalized on both NCs. In this configuration both one-site CM and two-site CM effects can occur. The label $d = \infty$ denotes a configuration where NCs are placed at a great distance.

systems of PbSe NCs.[46] In order to provide a microscopic interpretation of trends of Figures 2 and 3, we report calculated one- and two-site CM lifetimes for all the considered NC−NC separations (see Figure 4). At $d = 1$ nm, NC−NC interaction is weak, and wave functions are almost totally confined onto single NCs. In this configuration two-site CM events are slow, and the overall efficiency of the CM is only determined by the occurrence of one-site CM decay dynamics (see panels (a) and (b) of Figure 4). When NC−NC separation is reduced, wave functions start to delocalize on the entire system, and significant changes in both plots of one- and two-site CM lifetimes appear. Such changes are essentially due to the occurrence of new CM relaxation mechanisms that are forbidden when NCs interplay is turned off. When, for instance, a single state initially localized onto the $Si_{147}H_{100}$ (scheme (a) of Figure 5) spreads over the $Si_{293}H_{172}$, two new CM decay mechanisms are simultaneously activated. The first one is a one-site CM relaxation process generated in the large NC by the portion of state spilled from the small NC (scheme (b) of Figure 5). The second one is a two-site CM process (that shows CDCT character) ignited by the part of wave funtion still localized onto the small NC and that involves final states localized on the large NC (scheme (c) of Figure 5). Processes of this type are made possible by the sharing of wave functions among interacting NCs and are at the basis of the new points that emerge between $E^{th}_{Si_{293}H_{172}}$ and $E^{th}_{Si_{147}H_{100}}$ in plots of Figure 4. Obviously NC−NC interaction makes possible a large variety of two-site recombination mechanisms (see Figure 1, yellow and orange panels), that explains the large number of events recorded in the right panels of Figure 4. Such points, and the relative lifetimes, strongly depend on the carrier density localization and therefore on NC−NC separation. At $d = 1.0$ and $d = 0.8$ nm, Coulomb interaction between separated NCs is weak, and the transitions (one- and two-site) induced by NCs interplay are not sufficiently fast to modify existing relaxation dynamics. At $d = 0.6$ and especially $d = 0.4$, instead, NC−NC interaction (and thus wave function delocalization) becomes strong and induces new, fast one- and two-site CM relaxation paths that, especially at low energies, can intensify CM effects. As a fact, when NC−NC interaction is negligible, absorption of a photon with an energy between $E^{th}_{Si_{293}H_{172}} \div E^{th}_{Si_{147}H_{100}}$ can lead to CM effects only in the $Si_{293}H_{172}$. When the same photo-absorption process involves states of the $Si_{147}H_{100}$, the generated e−h pairs thermalize and recombine radiatively. On the contrary, for NCs placed in close proximity, excitations in

the range $E^{th}_{Si_{293}H_{172}} \div E^{th}_{Si_{147}H_{100}}$ can lead to CM effects when photons are absorbed either by the $Si_{293}H_{172}$ or by the $Si_{147}H_{100}$. Thanks to the spread of wave functions, both the $Si_{293}H_{172}$ and the $Si_{147}H_{100}$ play now an active role and can, in this window of energies, contribute to the CM dynamics. The final result is therefore an improvement of the CM effects at low energies that can lead to a reduction of the detectable CM energy threshold. At the same time, NCs interplay does not significantly modify the intensity of CM processes far from the CM threshold; here, one-site decay processes dominate CM effects, leading to the formation of Auger affected multiexciton configurations localized onto single NCs.

The occurrence of novel and efficient CM relaxation processes were hypothesized in ref 44 in order to explain results obtained in ultrafast pump−probe measurements conducted in a low pulse fluence regime on closely packed Si-NCs. In this experiment, similarities between exciton decay features observed for high- and low-energy excitations, and the missing of a fast degradation component in the IA signal for the above CM excitations, were explained by assuming the occurrence of two-site CM effects that, dominating CM dynamics, inhibit Auger recombination (AR) processes leading to a direct generation of multiexcitons distributed onto closely coupled Si-NCs. As previously noted, however, this interpretation is not compatible with our results.

On the basis of experimental findings[44] and on theoretical results,[37] we develop a simplified model in order to study the time evolution of the number of e−h pairs generated in a sample of closely packed Si-NCs upon absorption of high-energy photons. In order to interpret the experimental data and to motivate the missing of a fast decay component in the recorded IA signal, we reconsider the role played by AR that is here described as an active process and not solely as an ultimate mechanism that only kills the biexciton population. In particular high-energy carrier dynamics are simulated assuming that active CM configurations can be repopulated by biexciton AR. This procedure is defined Auger recycling and, from an initial biexciton configuration, leads to the formation of a single e−h pair that can again decay by fast (one- or two-site) CM. By implementing Auger recycling, one-site and two-site CM mechanisms in a system of coupled rate equations (see eq 5), and by adopting CM lifetimes calculated by ab initio methodologies,[37] we analyze the time evolution of the number of e−h pairs (and their localization) probed in a sample of strongly coupled Si-NCs after pump-pulse, when low pump fluence conditions are satisfied. In particular we calculate, as a
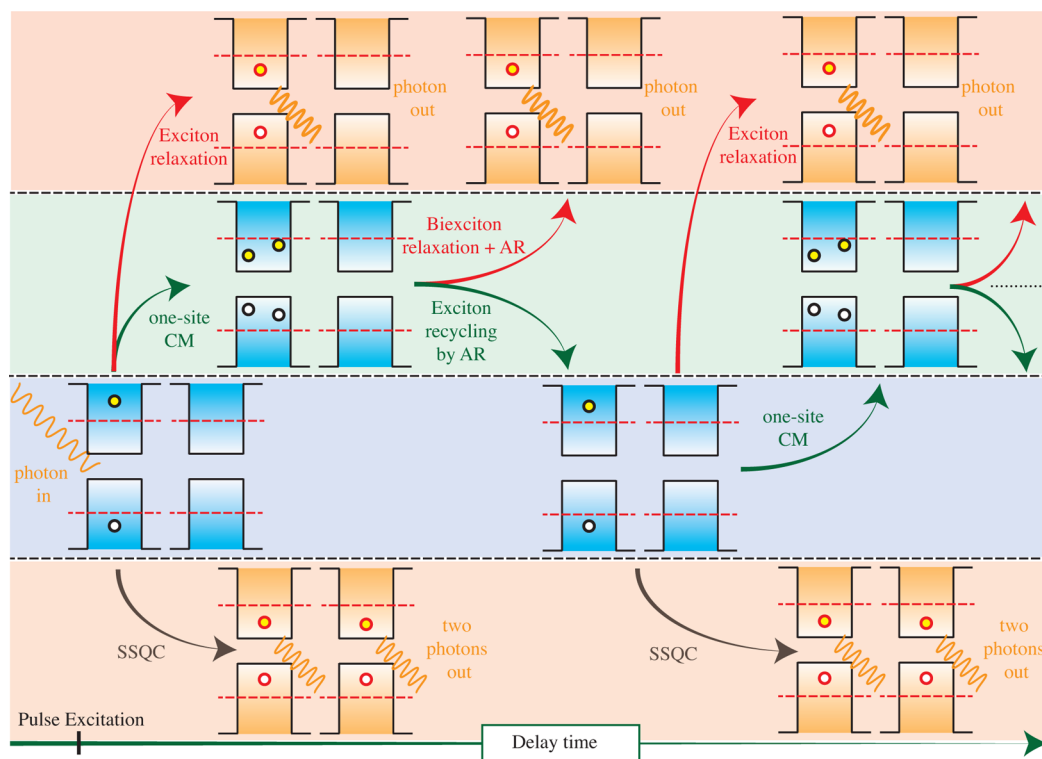
Figure 6. A schematic representation of the procedure implemented in eq 5. The high-energy exciton $X^\star$, generated after pulse excitation, can decay by one-site CM, generating a biexciton XX, by SSQC leading to single excitons $X + X$, or thermalize to X. The biexciton XX can then recycle an active configuration $X^\star$ by AR or relax and decay to X. The active configuration $X^\star$ can again decay by one-site CM, by SSQC or relax to X. The cyclic procedure stops when thermalization mechanisms make it impossible to restore an active configuration.

function of the time delay, the fraction of NCs with a biexciton (n_{XX}), with an above CM threshold exciton ($n_X^\star$) and with a below CM threshold exciton (n_X). In our model, an above CM energy threshold exciton ($X^\star$) is generated immediately after absorption of a high-energy photon. Using the calculated ab initio lifetimes of ref 37 and the procedure implemented in eq 5, the initial configuration is rapidly depopulated according to three different decay channels: by one-site CM leading to the formation of a biexciton XX, by SSQC leading to the formation of two excitons localized on space separated NCs ($X + X$), or by thermal relaxation leading to a single below CM threshold e−h pair X, subject to radiative decay only. While e−h pairs formed through the quantum cutting mechanisms are long-lived and subject to radiative recombination only, biexcitons undergo AR which, depending on the energy of XX, can lead to a quick regeneration of a new hot exciton $X^\star$, that can decay again by CM (Auger exciton recycling, $XX \rightarrow X^\star$), or to the formation of a single e−h pair X (Auger decay $XX \rightarrow X$) that thermalizes and recombines radiatively (in eq 5, the parameter f defines the fraction of $X^\star$ that are recycled from XX; in a realistic system this fraction depends on the ratio between biexciton relaxation and Auger recycling rates). This procedure, described in Figure 6, is cyclic and stops when loss factors inhibit the regeneration of single excitons with an energy sufficiently high to give rise again to fast CM processes, that is when relaxation mechanisms make impossible the transition $XX \rightarrow X^\star$.

$$
\begin{cases}
\dfrac{\mathrm{d}}{\mathrm{d}t}n_{X^\star} = -\left(\dfrac{1}{\tau_{\text{one-site}}} + \dfrac{1}{\tau_{\text{SSQC}}} + \dfrac{1}{\tau_{\text{relax}}}\right)n_{X^\star} \\[2mm]
\qquad\qquad + \dfrac{f}{\tau_{\text{Auger}}}n_{XX} \\[3mm]
\dfrac{\mathrm{d}}{\mathrm{d}t}n_{XX} = -\dfrac{1}{\tau_{\text{Auger}}}n_{XX} + \dfrac{1}{\tau_{\text{one-site}}}n_{X^\star} \\[3mm]
\dfrac{\mathrm{d}}{\mathrm{d}t}n_X = \left(\dfrac{2}{\tau_{\text{SSQC}}} + \dfrac{1}{\tau_{\text{relax}}}\right)n_{X^\star} - \dfrac{1}{\tau_{\text{radiative}}}n_X \\[3mm]
\qquad\qquad + \dfrac{1-f}{\tau_{\text{Auger}}}n_{XX}
\end{cases}
\tag{5}
$$

As previously noted, an exhaustive ab initio comprehension of thermalization processes in NCs is still missing; consequently, their inclusion in the present work is done in the form of a global effective lifetime (τ_{relax}). Noticeably, CDCT processes are not implemented in eq 5. These mechanisms lead to final configurations that are equivalent to the one produced by one-site CM. However, especially at high energies, one-site CM processes are faster than CDCT effects.[37] For this reason the implementation of CDCT, which requires complicating the structure of the rate equations, would not be conducive to significant changes in the model of eq 5, which is kept simple, neglecting this decay mechanism. Starting from effective Coulomb matrix elements and density of final states calculated by first-principles calculations,[54] we have estimated the lifetime for the process $XX \rightarrow X^\star$ that, for hydrogenated Si-NCs of about 2 nm of diameter, settles to about 1 ps. Noticeably, such
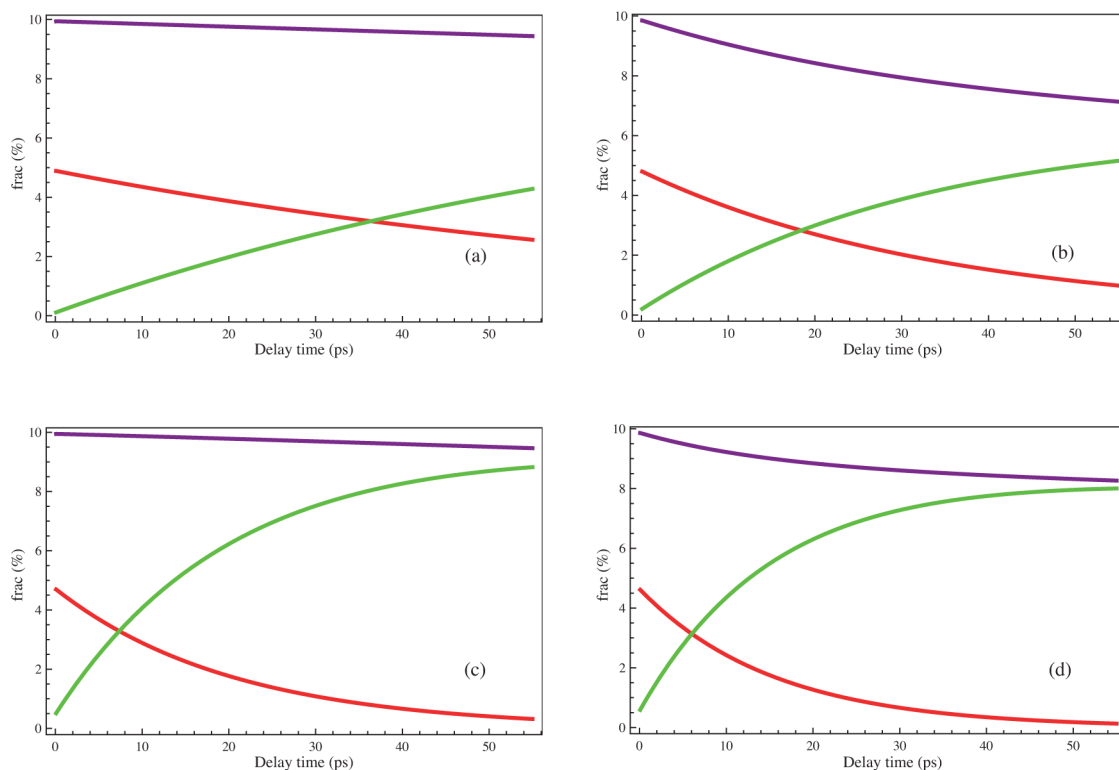
Figure 7. Solutions of eq 5. To simulate low-pulse excitations, we assume as an initial condition a population of the 5% of $X^\star$. Purple line denotes the total fraction of e−h pairs $(2n_{XX} + n_X^\star + n_X)$ generated in the sample after photons absorption. Red and green lines represent the fraction of biexciton XX and single excitons X as a function of the delay time. Calculations have been performed assuming $\tau_{one-site}$ = 0.01 ps, τ_{Auger} = 1 ps, and $\tau_{radiative}$ = 1000 ps. From panel (a) to panel (d) we have τ_{SSQC} = 1 ps and τ_{relax} = 5 ps, τ_{SSQC} = 1 ps and τ_{relax} = 0.5 ps, τ_{SSQC} = 0.2 ps and τ_{relax} = 5 ps, τ_{SSQC} = 0.2 ps and τ_{relax} = 0.5 ps. We assume here that the biexciton is always recycled (f = 1).

value must not be confused with the measured biexciton lifetime that instead refers to Auger decay dynamics that leads to a reduction of the number of e−h pairs in the sample. Auger recycling is a single-step process $XX \rightarrow X^\star$ that, in our model, is a part of complex dynamics. The Auger decay, instead, refers to a more complicated irreversible and detrimental process $XX \rightarrow X$. The possibility of repopulating biexciton configurations through a combination of Auger recycling and one-site CM processes yields the Auger decay to be not a straighforward process but instead the result of a multistep mechanism where thermalization processes concur as well. As a consequence, measured biexciton lifetimes represent an upper limit to the calculated Auger recycle lifetimes. Remarkably, a similar multistep vision of the Auger recombination (based also in this case on the presence of exciton recycling mechanisms) was also supposed in order to explain energy transfer dynamics in Er^{3+} doped Si-NCs.[55,56] In eq 5, $\tau_{one-site}$ and τ_{Auger} are the lifetimes associated with one-site CM decay processes and Auger recycle mechanisms, respectively. $\tau_{radiative}$ is introduced to describe radiative recombination mechanisms. The set of expressions of eq 5 are studied as a function of τ_{SSQC} and τ_{relax}, assuming $\tau_{one-site}$ = 0.01 ps[37] and τ_{Auger} = 1 ps and by setting $\tau_{radiative}$ = 1 ns. Numerical calculations pointed out that, for a system of hydrogenated and strongly interacting Si-NCs of about 2 nm of diameter, SSQC lifetimes settle to about 1 ps on a large scale of energies. However, NCs of larger size or differently passivated can have smaller SSQC lifetimes, so that 1 ps has to be considered as an upper limit for energy transfer quantum cutting mechanisms ignited by the relaxation of high-energy carriers. For this reason we analyze dynamics of eq 5 by

considering two different values of the parameter τ_{SSQC}, that is 1 and 0.2 ps, respectively. Again, we explore two different relaxation regimes, that is τ_{relax} = 5 ps and τ_{relax} = 0.5 ps (we consider therefore also subps relaxation mechanisms that could characterize non-CM relaxation dynamics at very high energies). When biexciton relaxation processes are significantly slower than exciton recycling procedures, biexcitons mainly relax by AR to $X^\star$ (f = 1). Results obtained by solving eq 5 assuming an initial $X^\star$ population of 5% (low pulse conditions) and imposing f = 1, are reported in Figure 7. Here, purple lines denote the total fraction of excitons generated in the sample $(n_{exc} = 2n_{XX} + n_X + n_X^\star)$, while red and green lines denote the fraction of biexciton (n_{XX}) and of below CM excitons (n_X) generated after pump pulse, respectively. From Figure 7, we observe that one-site CM is responsible for probing a double number of excitons with respect to the number of absorbed photons soon after (∼10 fs) the pulse excitation. The time evolution of n_{exc} is then determined by the repetitive combination of one-site CM, SSQC, and exciton recycling mechanisms. At the beginning biexciton population dominates (see red line). Then single excitons localized onto space-separated NCs emerge as a consequence of the recursive procedure implemented in eq 5 (see green line). After the crossing of red and green lines, it is more likely to have two excitons distributed on two separated NCs rather than a biexciton localized onto a well-defined NC (the crossing occurs at lower delay time when SSQC and relaxation processes become faster, and can occur in less than 10 ÷ 20 ps when τ_{SSQC} = 0.2 ps). Few tens of picoseconds (ps) after the pulse excitation, biexciton population is strongly reduced and rapidly
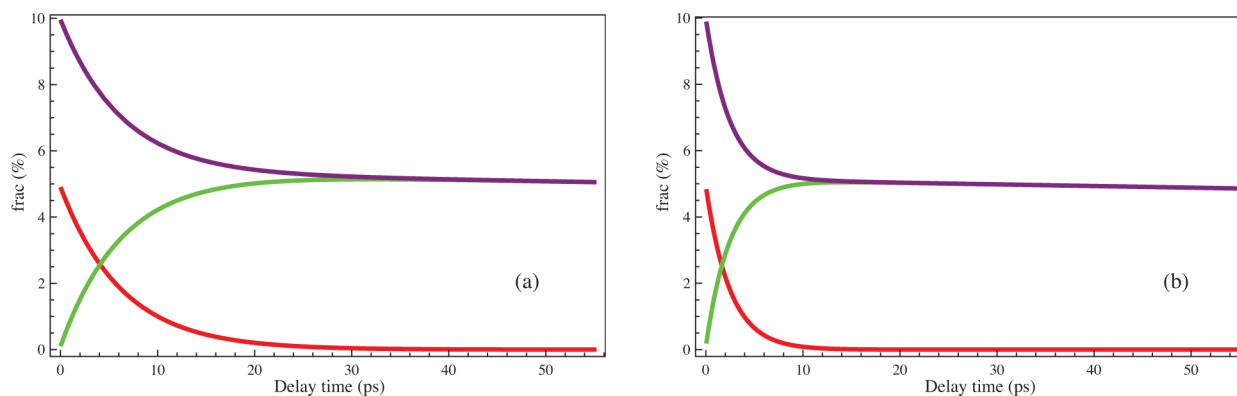
Figure 8. Solutions of eq 5. We assume $\tau_{SSQC} = 1$ ps and $\tau_{relax} = 5$ ps. In panel (a) we consider $f = 0.85$. In panel (b) $f = 0.60$.

moves to zero if SSQC processes fall in the subps scale. In this case the repetitive combination of one-site CM, SSQC, and Auger recycling is able to rapidly distribute a large part of the initially absorbed energy on space separated NCs, leading to the generation of long-lived configurations that are subjected to radiative decay only. Solutions of Figure 7 point out that the time evolution of the total fraction of e−h pairs generated after photon absorption depends on both SSQC and relaxation lifetimes. Anyway, for all considered cases, purple lines do not show fast decay components (in agreement with experiments of ref 44), despite our model where we do not assume suppression of the Auger recombination and we have the formation of multiexcitons onto single NCs. Results of Figure 7 have been obtained by considering the occurrence of very efficient recycling effects, that is by hypothesizing that recombination of biexcitons by Auger can always lead to the formation of active configuration $X^\star$ ($f = 1$). When this condition is not completely satisfied, a fast degradation in the number of e−h pairs generated after pump excitation emerges. This effect results from eq 5 by analyzing the case $f < 1$, that is by studying exciton dynamics in the hypothesis that only a fraction of biexcitons can recycle active $X^\star$ configurations. Results obtained by monitoring n_{exc} as a function of the delay time for $f = 0.85$ and $f = 0.60$ are reported in left and right panels of Figure 8 (for simplicity we consider only the case $\tau_{SSQC} = 1$ ps and $\tau_{relax} = 5$ ps). Here, a non-negligible decay component appears in the purple line already for $f = 0.85$, that is when only a small fraction of biexcitons are supposed to be unable to recycle configurations that can, again, decay by CM. This effect is even more evident for $f = 0.60$, proving that, in these conditions, effects induced by CM on e−h population are largely lost a few picoseconds after the excitation pulse. When $f < 1$, therefore, neither SSQC nor Auger recycling mechanisms are sufficient to explain results of ref 44, and a more complicated model has to be proposed.

CONCLUSIONS

In conclusion, we have calculated CM lifetimes for a system of two interacting Si-NCs. Our results point out that NCs interplay leads to an intensification of CM dynamics at low energies. This effect is strongly boosted by wave function delocalization and is originated by the occurrence of new CM effects which are forbidden in systems of noninteracting NCs. Due to the sharing of wave functions among different NCs, the small nanoparticles can participate in CM decay events also at energies below their own CM energy threshold. Our ab initio results point out that, when NCs are placed in close proximity,

effects induced by NCs interplay are sufficiently fast to modify CM dynamics at low energies and can lead to a reduction of the CM energy threshold. At the same time the intensity of CM dynamics is only weakly affected by NCs interplay when decays ignited by relaxation of high-energy carriers are considered. Effects induced by NC−NC interaction on the time evolution of the excited carriers are simulated by solving a set of rate equations where a cyclic procedure involving one-site CM processes, two-site CM effects, and exciton recycling mechanisms is proved to be compatible with ultrafast spectroscopy experiments conducted on dense arrays of Si-NCs.[42−44] Our model, that clearly reformulates the role played by AR that is here considered able to re-excite carriers to above CM threshold levels, points out that generation of multiexciton configurations distributed in space-separated NCs could be connected with the competition between Auger recycling mechanisms and thermalization processes and can occur when exciton recycling mechanisms are faster than biexciton relaxation dynamics. When this condition is not verified, our model is not sufficient to interpret results of ref 44, and a more complicated approach becomes necessary.

ASSOCIATED CONTENT

ⓢ Supporting Information

Methods and theory; spill-out parameter; atomic positions. This material is available free of charge via the Internet at http://pubs.acs.org.

AUTHOR INFORMATION

Corresponding Authors
marri@unimo.it
mgovoni@uchicago.edu

Present Address
#Institute for Molecular Engineering, the University of Chicago, 5555 South Ellis Avenue, Chicago, Illinois 60637, United States.

Notes
The authors declare no competing financial interest.

ACKNOWLEDGMENTS

the European Community Seventh Framework Programme (FP7/2007-2013; Grant Agreement 245977).

■ REFERENCES

(1) Ossicini, S.; Bisi, O.; Degoli, E.; Marri, I.; Iori, F.; Luppi, E.; Magri, R.; Poli, R.; Cantele, G.; Ninno, D.; Trani, F.; Marsili, M.; Pulci, O.; Olevano, V.; Gatti, M.; Gaal-Nagy, K.; Incze, A.; Onida, G. *J. Nanosci. Nanotechnol.* **2008**, *8*, 479.

(2) Degoli, E.; Guerra, R.; Iori, F.; Magri, R.; Marri, I.; Pulci, O.; Bisi, O.; Ossicini, S. *C. R. Phys.* **2009**, *10*, 575.

(3) Iori, F.; Degoli, E.; Luppi, E.; Magri, R.; Marri, I.; Cantele, G.; Ninno, D.; Trani, F.; Ossicini, S. *J. Lumin.* **2006**, *121*, 335−339.

(4) Guerra, R.; Marri, I.; Magri, R.; Martin-Samos, L.; Pulci, O.; Degoli, E.; Ossicini, S. *Phys. Rev. B* **2009**, *79*, 155320.

(5) Iori, F.; Degoli, E.; Magri, R.; Marri, I.; Cantele, G.; Ninno, D.; Trani, F.; Pulci, O.; Ossicini, S. *Phys. Rev. B* **2007**, *76*, 085302.

(6) Priolo, F.; Gregorkiewicz, T.; Galli, M.; Krauss, T. F. *Nat. Nanotechnol.* **2014**, *9*, 19−32.

(7) Nozik, A. J. *Inorg. Chem.* **2005**, *44*, 6893−6899 (PMID: 16180844).

(8) Ellingson, R. J.; Beard, M. C.; Johnson, J. C.; Yu, P.; Micic, O. I.; Nozik, A. J.; Shabaev, A.; Efros, A. L. *Nano Lett.* **2005**, *5*, 865−871.

(9) Schaller, R. D.; Klimov, V. I. *Phys. Rev. Lett.* **2004**, *92*, 186601.

(10) Trinh, M. T.; Houtepen, A. J.; Schins, J. M.; Hanrath, T.; Piris, J.; Knulst, W.; Goossens, A. P. L. M.; Siebbeles, L. D. A. *Nano Lett.* **2008**, *8*, 1713−1718 (PMID: 18489170).

(11) Klimov, V. I. *J. Phys. Chem. B* **2006**, *110*, 16827−16845 (PMID: 16927970).

(12) Klimov, V. I. *Appl. Phys. Lett.* **2006**, *89*, 123118.

(13) Nair, G.; Bawendi, M. G. *Phys. Rev. B* **2007**, *76*, 081304.

(14) Nozik, A. J. *Chem. Phys. Lett.* **2008**, *457*, 3−11.

(15) Schaller, R. D.; Petruska, M. A.; Klimov, V. I. *Appl. Phys. Lett.* **2005**, *87*, 253102.

(16) Schaller, R. D.; Sykora, M.; Pietryga, J. M.; Klimov, V. I. *Nano Lett.* **2006**, *6*, 424−429 (PMID: 16522035).

(17) Beard, M. C.; Midgett, A. G.; Hanna, M. C.; Luther, J. M.; Hughes, B. K.; Nozik, A. J. *Nano Lett.* **2010**, *10*, 3019−3027.

(18) Nootz, G.; Padilha, L. A.; Levina, L.; Sukhovatkin, V.; Webster, S.; Brzozowski, L.; Sargent, E. H.; Hagan, D. J.; Van Stryland, E. W. *Phys. Rev. B* **2011**, *83*, 155302.

(19) Semonin, O. E.; Luther, J. M.; Choi, S.; Chen, H.-Y.; Gao, J.; Nozik, A. J.; Beard, M. C. *Science* **2011**, *334*, 1530−1533.

(20) Califano, M.; Zunger, A.; Franceschetti, A. *Appl. Phys. Lett.* **2004**, *84*, 2409−2411.

(21) Schaller, R. D.; Sykora, M.; Jeong, S.; Klimov, V. I. *J. Phys. Chem. B* **2006**, *110*, 25332−25338 (PMID: 17165979).

(22) Gachet, D.; Avidan, A.; Pinkas, I.; Oron, D. *Nano Lett.* **2010**, *10*, 164−170 (PMID: 19911830).

(23) Murphy, J. E.; Beard, M. C.; Norman, A. G.; Ahrenkiel, S. P.; Johnson, J. C.; Yu, P.; Mićić, O. I.; Ellingson, R. J.; Nozik, A. J. *J. Am. Chem. Soc.* **2006**, *128*, 3241−3247 (PMID: 16522105).

(24) Pijpers, J. J. H.; Hendry, E.; Milder, M. T. W.; Fanciulli, R.; Savolainen, J.; Herek, J. L.; Vanmaekelbergh, D.; Ruhman, S.; Mocatta, D.; Oron, D.; Aharoni, A.; Banin, U.; Bonn, M. *J. Phys. Chem. C* **2007**, *111*, 4146−4152.

(25) Schaller, R. D.; Pietryga, J. M.; Klimov, V. I. *Nano Lett.* **2007**, *7*, 3469−3476.

(26) Stubbs, S. K.; Hardman, S. J. O.; Graham, D. M.; Spencer, B. F.; Flavell, W. R.; Glarvey, P.; Masala, O.; Pickett, N. L.; Binks, D. J. *Phys. Rev. B* **2010**, *81*, 081303.

(27) Beard, M. C.; Knutsen, K. P.; Yu, P.; Luther, J. M.; Song, Q.; Metzger, W. K.; Ellingson, R. J.; Nozik, A. J. *Nano Lett.* **2007**, *7*, 2506−2512.

(28) McGuire, J. A.; Joo, J.; Pietryga, J. M.; Schaller, R. D.; Klimov, V. I. *Acc. Chem. Res.* **2008**, *41*, 1810−1819.

(29) McGuire, J. A.; Sykora, M.; Joo, J.; Pietryga, J. M.; Klimov, V. I. *Nano Lett.* **2010**, *10*, 2049−2057 (PMID: 20459066).

(30) Midgett, A. G.; Hillhouse, H. W.; Hughes, B. K.; Nozik, A. J.; Beard, M. C. *J. Phys. Chem. C* **2010**, *114*, 17486−17500.

(31) Califano, M.; Zunger, A.; Franceschetti, A. *Nano Lett.* **2004**, *4*, 525−531.

(32) Allan, G.; Delerue, C. *Phys. Rev. B* **2006**, *73*, 205423.

(33) Franceschetti, A.; An, J. M.; Zunger, A. *Nano Lett.* **2006**, *6*, 2191−2195.

(34) Luo, J.-W.; Franceschetti, A.; Zunger, A. *Nano Lett.* **2008**, *8*, 3174−3181.

(35) Allan, G.; Delerue, C. *Phys. Rev. B* **2009**, *79*, 195324.

(36) Rabani, E.; Baer, R. *Nano Lett.* **2008**, *8*, 4488−4492.

(37) Govoni, M.; Marri, I.; Ossicini, S. *Nat. Photonics* **2012**, *6*, 672−679.

(38) Vörös, M.; Rocca, D.; Galli, G.; Zimanyi, G. T.; Gali, A. *Phys. Rev. B* **2013**, *87*, 155402.

(39) Schaller, R. D.; Agranovich, V. M.; Klimov, V. I. *Nat. Phys.* **2005**, *1*, 189−194.

(40) Rabani, E.; Baer, R. *Chem. Phys. Lett.* **2010**, *496*, 227−235.

(41) Shabaev, A.; Efros, A. L.; Nozik, A. J. *Nano Lett.* **2006**, *6*, 2856−2863.

(42) Timmerman, D.; Izeddin, I.; Stallinga, P.; YassievichI, N.; Gregorkiewicz, T. *Nat. Photonics* **2008**, *2*, 105−109.

(43) Timmerman, D.; Valenta, J.; Dohnalova, K.; de Boer, W. D. A. M.; Gregorkiewicz, T. *Nat. Nanotechnol.* **2011**, *6*, 710−713.

(44) Trinh, M. T.; Limpens, R.; de Boer, W. D. A. M.; Schins, J. M.; Siebbeles, L. D. A.; Gregorkiewicz, T. *Nat. Photonics* **2012**, *6*, 316−321.

(45) Aerts, M.; Suchand Sandeep, C. S.; Gao, Y.; Savenije, T. J.; Schins, J. M.; Houtepen, A. J.; Kinge, S.; Siebbeles, L. D. A. *Nano Lett.* **2011**, *11*, 4485−4489.

(46) Sandeep, C. S. S.; Cate, S.; Schins, J. M.; Savenije, T. J.; Liu, Y.; Law, M.; Kinge, S.; Houtepen, A. J.; Siebbeles, L. D. A. *Nat. Commun.* **2013**, *4*, 2360.

(47) Govoni, M.; Marri, I.; Ossicini, S. *Phys. Rev. B* **2011**, *84*, 075215.

(48) Marini, A.; Hogan, C.; Grüning, M.; Varsano, D. *Comput. Phys. Commun.* **2009**, *180*, 1392−1403.

(49) Allan, G.; Delerue, C. *Phys. Rev. B* **2008**, *77*, 125340.

(50) Stewart, J. T.; Padilha, L. A.; Bae, W. K.; Koh, W.-K.; Pietryga, J. M.; Klimov, V. I. *J. Phys. Chem. Lett.* **2013**, *4*, 2061−2068.

(51) Padilha, L. A.; Stewart, J. T.; Sandberg, R. L.; Bae, W. K.; Koh, W.-K.; Pietryga, J. M.; Klimov, V. I. *Acc. Chem. Res.* **2013**, *46*, 1261−1269.

(52) de Boer, W. D. A. M.; Timmerman, D.; Dohnalova, K.; Yassievich, I. N.; Zhang, H.; Buma, W. J.; Gregorkiewicz, T. *Nat. Nanotechnol.* **2010**, *5*, 878−884.

(53) Moskalenko, A. S.; Berakdar, J.; Poddubny, A. N.; Prokofiev, A. A.; Yassievich, I. N.; Goupalov, S. V. *Phys. Rev. B* **2012**, *85*, 085432.

(54) Coulomb matrix elements adopted in the calculation of Auger lifetimes are the same used to calculate CM lifetimes.

(55) Navarro-Urrios, D.; Pitanti, A.; Daldosso, N.; Gourbilleau, F.; Rizk, R.; Garrido, B.; Pavesi, L. *Phys. Rev. B* **2009**, *79*, 193312.

(56) Pitanti, A.; Navarro-Urrios, D.; Prtljaga, N.; Daldosso, N.; Gourbilleau, F.; Rizk, R.; Garrido, B.; Pavesi, L. *J. Appl. Phys.* **2010**, *108*, 053518.